

Density structure in low-order harmonic emission from laser-plasma interactions

T.J.M. Boyd

*Centre for Physics, University of Essex,
Wivenhoe Park, Colchester CO4 3SQ, Essex, UK*

R. Ondarza-Rovira

*Instituto Nacional de Investigaciones Nucleares,
Apartado Postal 18-1027, México 11801, D.F.*

Recibido el 7 de julio de 2005; aceptado el 6 de marzo de 2006

Multiple harmonic generation from intense laser light incident on dense plasma targets is well-established. Both the number of harmonics generated and the corresponding power in each is strongly dependent on the intensity of the incident light. In this paper, attention is focused on an aspect of harmonic generation that has hitherto been largely overlooked, namely its dependence on plasma density. In particular we show that the conversion efficiencies of odd harmonics generated for normally incident light are strongly resonant in character, the number of resonances increasing with harmonic order. In addition to this resonant behaviour, the reflected power in low-order harmonics is further complicated by plasma emission at plasma resonant densities. Only at densities well above the resonances does the radiated harmonic power decay monotonically with density. The density dependence predicted by theory for low-order harmonics is confirmed by particle-in-cell simulations.

Keywords: Laser-plasma interaction; high harmonic generation.

La generación de armónicos a partir de la interacción de luz láser intensa en plasmas densos ha sido ampliamente estudiada. Tanto el número de armónicos generados como la potencia emitida dependen fuertemente de la intensidad de la luz incidente. En este trabajo se da particular atención a un aspecto de la generación de armónicos que hasta ahora no ha sido considerado, a saber su dependencia con la densidad del plasma. En particular, mostramos que las eficiencias de conversión de armónicos impares generados por incidencia normal se caracterizan por ser fuertemente resonantes, el número de resonancias aumenta con el orden del armónico emitido. Además de este comportamiento resonante, la potencia reflejada en los armónicos de bajo orden es adicionalmente combinado por emisión del plasma en las densidades de plasma resonante. Sólo en las densidades por arriba de las resonancias la potencia radiada de los armónicos decae monótonamente con la densidad. La dependencia con la densidad predicha por la teoría para armónicos de bajo orden se confirma a través de la simulación numérica de partículas.

Descriptores: Interacción plasma-láser; generación de armónicos.

PACS: 52.40.Nk; 52.50.Jm; 52.65.Rr

1. Introduction

Much attention has been paid to aspects of the interaction of intense laser light with solid-density targets in which the plasma is overdense in terms of the critical density. In large part, this activity has been driven by the need to understand effects such as channel formation and the acceleration of ions and electrons to relativistic energies that have a direct bearing on what is known as the fast ignition approach to inertial fusion. Alongside this, there has been renewed interest in effects well known from more benign regions of parameter space. One of the most enduring of these is harmonic generation and the generation of high harmonics of the incident laser light in particular. The first observations of this were recorded as long ago as 1977 by Burnett *et al.* [1] and subsequently by Carman *et al.* [2], using long pulse CO₂ laser light with wavelength 10.6 μm. These studies were extended into the short pulse regime by Norreys *et al.* [3] using 2.5 ps pulses with intensities up to 10¹⁹ W cm⁻², generating more than 70 harmonics. At high intensities, the power in the harmonics decayed only slowly with harmonic number m . Norreys *et al.* estimated that the power in the 38th harmonic (at 28 nm) was 24 MW. These observations were

in broad agreement with particle-in-cell (PIC) simulations of harmonic generation by Gibbon [4]. The ability to generate about 60 harmonics with power efficiencies $P_m/P_1 \geq 10^{-6}$ prompted speculation that high harmonics might provide a source of coherent MW x-rays.

By and large, the generation of multiple harmonics of intense laser light incident on an overdense plasma slab, and its spectral characteristics, are reasonably well understood. In the most general terms the spectrum is governed by two parameters, the photon and electron densities. The incident irradiance measured by $I \lambda_L^2$, where I denotes the intensity of light of wavelength λ_L , must be high enough to generate high harmonic numbers, while the plasma density needs to be significantly overdense for the high harmonics themselves to be sufficiently intense. A convenient index characterizing the interaction of laser light with the plasma electrons is the dimensionless quiver velocity $a_0 = 0.85(I_{18} \lambda_L^2)^{1/2}$, where I_{18} denotes intensity in units of 10¹⁸ W cm⁻² and λ_L is the wavelength of the incident light in microns. The criterion for plasma to be overdense is that the electron density n_e should be greater than the critical density $n_c = 1.1 \times 10^{21} \lambda_L^{-2} \text{cm}^{-3}$, with λ_L measured in microns.

In this paper we have used a cold plasma model to determine low-order ($m = 3, 5$) harmonic emission from a slab plasma, supplemented by a PIC code to obtain the power emitted at higher orders. In addition, we have made use of a simple scaling that allows us to estimate power levels in higher harmonics $P_{(2m+1)}$ for $m = 2, 3 \dots$ using PIC output for P_3 .

The harmonic dependence on a_0 is straightforward and broadly understood. For $a_0 \ll 1$ only low harmonic orders are excited; but as $a_0 \rightarrow 1$, the picture changes with a greatly extended harmonic range. There is no generally valid theoretical interpretation of high harmonic generation. An empirical expression due to Gibbon [4] suggests that for sufficiently large harmonic index m , the efficiency of harmonic generation scales as $(2a_0)^4/m^5$. One shortcoming of this empirical scaling is that it is determined solely as a function of laser intensity, although Gibbon elsewhere [5] acknowledges that one should expect some weak dependence on density and angle of incidence. Recent work by Gordienko *et al.* [6] presents an alternative scaling, namely a power-law harmonic spectrum decaying as m^{-p} , where $p = 5/2$ for a quasi-monochromatic incident laser pulse or $p = 3$ for a broadband pulse. However, this scaling is limited to a harmonic range that satisfies the condition $m < 4\gamma^2$, where γ is the maximum relativistic factor at the plasma boundary. Consequently there is little overlap between this work and that presented here which is restricted to a quasi-relativistic regime.

Our main purpose in this paper is to draw attention to the fact that harmonic emission may in fact be rather strongly dependent on density. This dependence comes from two distinct sources, each strongly resonant. The first has its origins in the sequence of cold plasma resonances [7] in the perturbed surface plasma density at $n_e/n_c = 4, 16, \dots (2m)^2$. The second density-dependent feature is emission from Langmuir waves excited at the plasma surface at the corresponding resonant densities by fluxes of electrons penetrating the plasma. The Langmuir waves couple to the radiation field in the steep density gradient at the plasma surface and contribute to the harmonic spectrum for densities $n_e = m^2 n_c$. Boyd and Ondarza [8] showed that this Langmuir wave radiation could affect the line spectrum significantly, especially in the region of low harmonics, where the blue wing of the plasma line may be strong enough to envelop the harmonic lines in its neighbourhood.

Of necessity, our perturbation model is limited to just first and second orders P_3 and P_5 , though it is possible to make estimates of reflected power levels at higher orders by means of a simple scaling. By considering only light normally incident on a plane plasma slab, we avoid geometrical complications associated with oblique incidence, even though the harmonic spectrum in consequence is limited to just odd harmonics. Restricting the range of a_0 to values ≤ 1 allows us to make use of a quasi-relativistic perturbation model, which is adequate for the purpose in hand. In any event, this restriction is needed if the assumption of a plane plasma surface is to hold

for the duration of the pulse. For high enough laser intensities ($a_0 \geq 1$), surface dimpling and subsequent channel formation within the target becomes a factor, often with rippled plasma surfaces, which is at variance with our assumption of normally incident light.

2. Model

Our model is that used in earlier studies of harmonic generation from overdense plasmas by Wilks, Kruer and Mori [9] in which linearly polarized light propagates in the z -direction and is incident on a plasma slab where the ions are taken as stationary, providing a uniform neutralizing background for the electrons. The electron density $n_e > n_c$ and the electron dynamics are described by the cold fluid equations, since the electron quiver velocity $\beta_\perp = \frac{a_\perp}{\gamma}$ is much greater than the thermal velocity. Here, $a_\perp(z, t) = e A_\perp / m_0 c^2$ is the normalized vector potential and e, m_0 the electron charge and rest mass. The normalized vector potential is determined by the wave equation

$$\square_z^2 \mathbf{a}_\perp = k_p^2 \frac{n_e}{n_0} \beta_\perp = k_p^2 \frac{n_e}{n_0} \frac{\mathbf{a}_\perp}{\gamma}, \quad (1)$$

in which

$$k_p = \omega_p / c, \omega_p^2 = 4\pi n_0 e^2 / m_0$$

and

$$\beta_\perp = \mathbf{v}_\perp / c = \mathbf{a}_\perp / \gamma$$

is the transverse electron fluid velocity normalized to the velocity of light, $\square_z^2 \equiv \frac{\partial^2}{\partial z^2} - \frac{1}{c^2} \frac{\partial^2}{\partial t^2}$. The relativistic mass factor γ is defined by

$$\gamma = (1 - \beta_\perp^2 - \beta_z^2)^{-1/2} = \frac{(1 + a_\perp^2)^{1/2}}{(1 - \beta_z^2)^{1/2}}. \quad (2)$$

The normalized scalar potential $\Phi = e \phi / m_0 c^2$ is determined by Poisson's equation

$$\frac{\partial^2 \Phi}{\partial z^2} = k_p^2 \left(\frac{n_e}{n_0} - 1 \right). \quad (3)$$

Harmonic generation is governed by the source term in (1) in which nonlinearity is introduced through the density n_e on the one hand and the relativistic mass factor on the other. The oscillating density is driven by the $\mathbf{v} \times \mathbf{B}$ force, which varies as a_\perp^2 and so introduces just even harmonics of a_\perp . Since this is also true for γ , it follows that the source term in (1) generates just odd harmonics. Even harmonics only appear in the spectrum, if we relax the constraint of normal incidence. Since our objective here is limited to highlighting the effect of the plasma density on the harmonic spectrum we confine our attention to low-order odd harmonics.

The relativistic cold fluid dynamic equations complete the set:

$$\frac{\partial n_e}{\partial t} + c \frac{\partial}{\partial z} (n_e \beta_z) = 0, \quad (4)$$

$$\frac{d\beta_z}{dt} = -\frac{1}{\gamma^2} \left[c \frac{\partial}{\partial z} + \beta_z \frac{\partial}{\partial t} \right] \frac{a_{\perp}^2}{2} + \frac{c}{\gamma} (1 - \beta_z^2) \frac{\partial \phi}{\partial z}. \quad (5)$$

A fully consistent treatment would include an evolution equation for the relativistic mass factor, but we exclude this from the present discussion. The procedure is then to adopt a perturbation expansion representing $a_{\perp} = a_0 + \epsilon a_3 + \epsilon^2 a_5 + O(\epsilon^3)$, where a_3, a_5 denote the vector potentials associated with the third and fifth harmonics. The corresponding density perturbation expansion is $n(z, t) = n_0 + \epsilon n_1(z, t) + \epsilon^2 n_2(z, t) + O(\epsilon^3)$. To first order we make use of the continuity equation (4) discarding the term $v_z \partial n_0 / \partial z$, which is responsible for oscillations of the plasma surface, together with (3) and (5) to obtain an equation governing the behaviour of n_1 , *i.e.*

$$\frac{\partial^2 n_1}{\partial t^2} + \omega_p^2 n_1 = \frac{n_0 c^2}{2} \frac{\partial^2 a_0^2}{\partial z^2}. \quad (6)$$

Note that in this ordering, $a_0^2 \sim \epsilon$. Since we are concerned with overdense plasmas such that $\omega_p \gg \omega_0$, by far the greater part of the incident light is reflected from the plasma surface. The transmitted fraction of the vector potential a_{\perp} decays within a skin depth of extent δ that is much smaller than λ_L . The sources generating the spectrum of harmonics are localized at the surface. Thus in (6) we need the form of the transmitted vector potential within this surface layer, a_{0t} . This is found by matching potential amplitudes and their z -derivatives at $z = 0$. For normal incidence this reduces to

$$a_{0t} = 2 \left(\frac{\omega_0}{\omega_p} \right) a_0 \exp(-z/\delta) \cos(-\omega_0 t + \phi), \quad (7)$$

with

$$\delta = \frac{c}{\omega_p} \left(1 - \frac{\omega_0^2}{\omega_p^2} \right)^{-1/2}$$

and

$$\tan \phi = \frac{\omega_0}{\omega_p} \left(1 - \frac{\omega_0^2}{\omega_p^2} \right)^{-1/2}.$$

With this representation in (6), we see that the source term on the right hand side is driven at $2\omega_0$, corresponding to the frequency of oscillation of the ponderomotive force. Moreover, the solution of (6) with the form for a_{0t} in (7) shows a cold plasma resonance at $\omega_p^2 = 4\omega_0^2$. Although this is the only source of third harmonic emission described by this model, we shall see from the PIC spectra that there is a significant contribution to third harmonic emission from the excitation of Langmuir waves near the plasma surface driven by electrons with a net drift in the z -direction. In the cold

plasma limit, the equation describing third harmonic generation becomes

$$(\square_z^2 - k_p^2) a_3 \simeq \frac{3 k_p^2 \omega_0^2 a_0^3}{\omega_p^2 - 4\omega_0^2} e^{-3z/\delta} \cos 3\omega_0 t. \quad (8)$$

This has the form of the Klein-Gordon equation with a small nonlinear term, and a solution was obtained using a Krylov-Bogoliubov procedure (Ondarza [10]). For present purposes, it is adequate and less laborious to integrate the source in (8) over a Green function, which results in

$$a_3 \simeq \frac{3}{8} \left(\frac{\omega_0}{\omega_p} \right) \frac{a_0^3}{\left(1 - 4 \frac{\omega_0^2}{\omega_p^2} \right)},$$

so that the power scaling for the third harmonic relative to power in the incident wave is then

$$\frac{P_3}{P_1} = \left(\frac{9}{8} \right)^2 \left(\frac{\omega_0}{\omega_p} \right)^2 \frac{a_0^4}{\left(1 - 4 \frac{\omega_0^2}{\omega_p^2} \right)^2}. \quad (9)$$

Since the ordering in our perturbation scheme took a_0^2 to be of the same order as n_1 , the expression in (9) gives non-physical levels for the reflected power for large a_0 . This is a consequence of the quasi-relativistic approximation used here. In reality, a proper, fully-relativistic model might be expected to introduce into (9) a denominator of the form $(1 + a_0^2/2)^p$, with $p \geq 2$. We have arbitrarily chosen $p = 3$, which is the form for the corresponding power in the case of an under-dense plasma first obtained by Sprangle *et al.* [11]. This at least has the merit of giving levels of P_3 emission that accord with those found from the PIC simulations in Sec. 3.

The supra-critical density condition $\omega_p^2 \gg \omega_0^2$ means that we can consider (9) as a reliable approximation for densities above $2n_c$, which avoids the cold plasma resonance implicit in (9). Remember too that, with increasing plasma density, the need to allow for significant nonlinear corrections is relaxed from $a_0 \geq 1$ to $a_0 (2\omega_0/\omega_p) > 1$ (cf. (7)). Physically this comes about because the overdense plasma effectively shields out the incident laser electric field, with the result that the quiver velocity is reduced by a factor $(2\omega_0/\omega_p)$ from the underdense case.

2.1. Numerical simulations

The PIC code used was a 1-1/2D electromagnetic, fully relativistic code with immobile ions, which serve as a neutralizing background. The plasma filled a simulation box extending over 6 laser wavelengths and containing 2×10^6 particles, sufficient to resolve a Debye length with acceptable resolution. Vacuum gaps were attached to both the front and rear plasma surfaces to allow for particle and wave propagation. The electromagnetic laser fields were launched at the front of the vacuum-plasma interface at normal incidence, with the plasma characterised by a sharp density profile with a scale length of only a fraction of a wavelength and then kept constant overdense. This representation of interaction conditions

at the front of the plasma slab is consistent with the assumptions of the proposed cold fluid model for the mechanism of harmonic generation when resonance absorption takes place in a highly steepened plasma density profile. The electron temperature was taken as 1 keV. Collisions between particles may be neglected for the simulation parameters used for input laser intensities, time scales and the highly steepened plasma interface. The harmonic power emission is obtained from the power spectral density, which in turn is determined using the data set of the time-integrated reflected electric field at the vacuum gap at the front of the plasma slab, by means of a fast Fourier transform. The reflected emission spectra showing the relative strength of the different oscillation modes is determined from the harmonic contents of the field, normalised to the fundamental.

3. Results

3.1. Third harmonic emission

In Fig. 1, we show P_3/P_1 for $0.1 < a_0 < 2$ and $n_e/n_c = 20$. With this choice, the agreement between the result from (9) and the PIC simulation points is satisfactory. The corresponding power ratio found by Wilks, Kruer and Mori [9], $P_3/P_1 \sim 0.1 a_0^4 (\omega_0/\omega_p)^4$, with a different density dependence, would appear to underestimate the power in third harmonic emission.

Since the emphasis in this paper is on plasma density effects on low harmonic generation we show in Fig. 2 how third harmonic emission depends on density in our model with PIC emission levels shown for comparison. The data shown correspond to a mildly relativistic case respond to a mildly relativistic case with $a_0 = 0.6$ across a density range up to $n_e = 100 n_c$. The theoretical result from (9) is plotted with a formal damping applied to resolve the cold plasma $n_e = 4 n_c$. The first point to note is the reasonable agreement

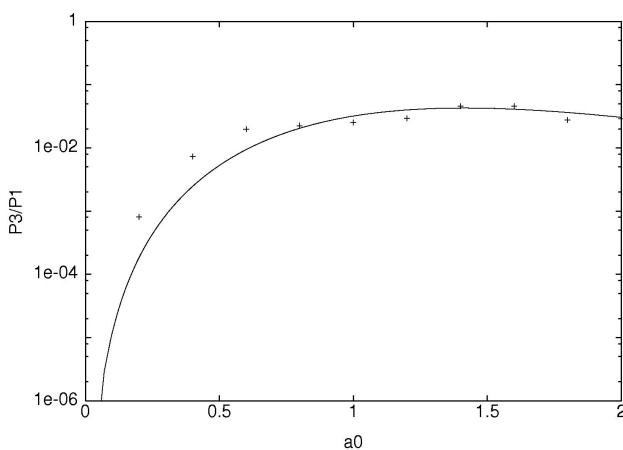


FIGURE 1. Reflected power in the third harmonic as a function of a_0 , for $n_e/n_c = 20$. The solid line denotes the cold plasma model result from (9). The points + were obtained from PIC simulations.

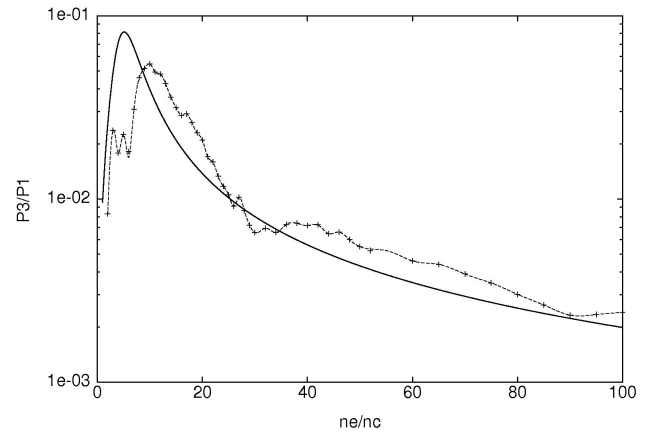


FIGURE 2. Reflected power in the third harmonic as a function of n_e/n_c , for $a_0 = 0.6$. The solid line denotes the cold plasma model result from (9) (with phenomenological damping added). The points + were obtained from PIC simulations.

between the density dependence from (9) with that shown by the PIC points, notably for $n_e \geq 30 n_c$. With this choice for a_0 , the corresponding values P_3/P_1 found by Wilks, Kruer and Mori [9] fall in the range $10^{-4} - 10^{-6}$.

As one would expect, the PIC data show a richer structure in the dependence of the third harmonic emission on density compared with the limited dependence contained in the theoretical model. In fact the resonance contained in (9) is only rather weakly represented in the PIC output in which the dominant feature is the strong third harmonic emission from the plasma for densities in the range of the corresponding Langmuir frequency ($n_e \sim 9 n_c$). Indeed, plasma emission, which is not included in our theoretical model, in all likelihood contributes to the P_3 emission in Fig. 2 at densities above $9 n_c$. There is, for example, some suggestion of P_3 enhancement at $n_e \sim 16 n_c$, $n_e \sim 25 n_c$ and $n_e \sim 36 n_c$ for which the corresponding Langmuir frequencies are $\omega_L \sim 4\omega_0$, $5\omega_0$ and $6\omega_0$. Plasma emission at these densities could then contribute to P_3 emission by means of parametric combinations (ω_L, ω_0) , $(\omega_L, 2\omega_0)$ and $(\omega_L, 3\omega_0)$. Note that above the region dominated by plasma line emission, the weak dependence of the third harmonic power on density found in (9) agrees reasonably well with the PIC result.

3.2. Fifth harmonic emission

Turning to the next order in our perturbation scheme, we obtained an expression for the power emitted in the fifth harmonic. The result found for P_5/P_1 is unwieldy, and we have rather arbitrarily excluded some unimportant contributions which amount to discarding non-resonant terms in the density perturbations to obtain a simplified form for P_5/P_1 . Applying a renormalization factor in this case as well to prevent nonphysical values for P_5/P_1 for $a_0 > 1$, again arbitrarily choosing the equivalent form from the under-dense results of Sprangle *et al.* [12], our result reduces to

$$\frac{P_5}{P_1} \simeq 0.55 \frac{\left(\frac{\omega_0}{\omega_p}\right)^2 \left(1 - \frac{9}{4} \frac{\omega_0^2}{\omega_p^2}\right)^2}{\left(1 - 4 \frac{\omega_0^2}{\omega_p^2}\right)^2 \left(1 - 16 \frac{\omega_0^2}{\omega_p^2}\right)^2} \frac{a_0^8}{\left(1 + \frac{a_0^2}{2}\right)^6}. \quad (10)$$

The combined limitations of the perturbation model with the relativistic normalization introduced mean that (10) should be seen as at best an estimate of power reflected in the fifth harmonic. In particular, no physical significance should be attached to the apparent cutoff introduced by the term in the numerator; this is prevented by a lower order contribution neglected for the convenience of writing a compact expression for P_5 . The key point in (10) is the appearance of an additional density resonance at $n_e = 16 n_c$ on top of the P_3 resonance at $n_e = 4 n_c$.

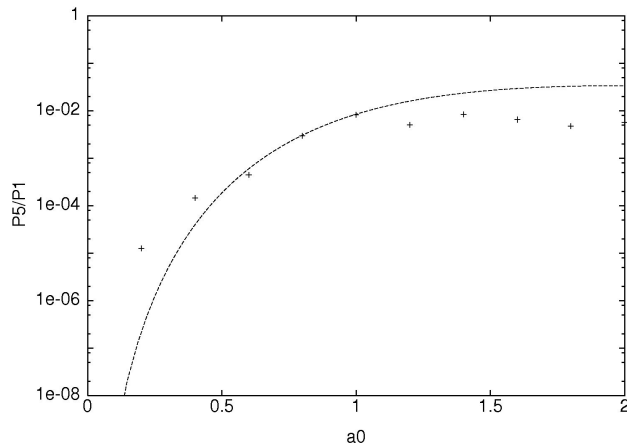


FIGURE 3. Reflected power in the fifth harmonic as a function of a_0 , for $n_e/n_c = 30$. The solid line denotes the cold plasma model result from (10). The points + were obtained from PIC simulations.

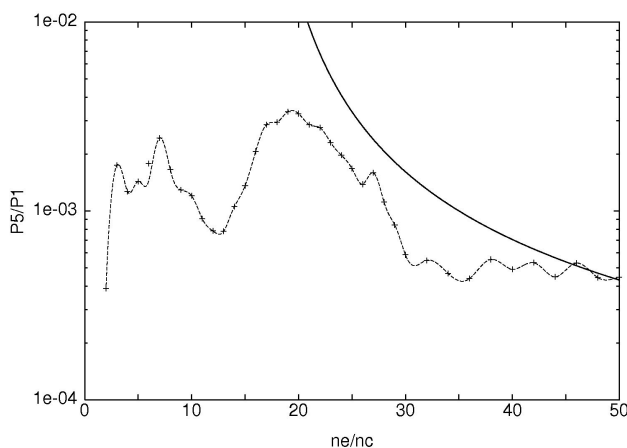


FIGURE 4. Reflected power in the fifth harmonic as a function of n_e/n_c , for $a_0 = 0.6$. The solid line denotes the cold plasma model result from (10). The points + were obtained from PIC simulations.

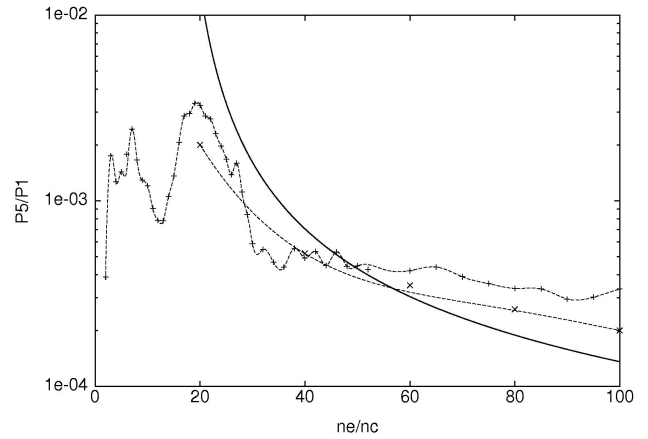


FIGURE 5. Reflected power in the fifth harmonic as a function of n_e/n_c , for $a_0 = 0.6$. The solid line denotes the cold plasma model result from (10) while the dashed line shows the estimated result from (11). The points + were obtained from PIC simulations.

Figure 3 shows (10) with the corresponding PIC points. A density $n_e = 30 n_c$ was chosen for this comparison to be far enough removed from the resonance at $n_e = 16 n_c$. Given the limitations of our analysis, the result is surprisingly robust, giving fair agreement with PIC results across the range.

Figure 4 shows P_5/P_1 as a function of the plasma density. On account of the strongly resonant nature of the expression in (10), we show the theoretical results above the resonant range. We see from this that the dependence on density is in good agreement with the PIC results only across a restricted density range. The PIC output shows two distinct resonances that broadly correspond to the structures predicted by (10). Not unexpectedly, they show a more complex structure with strong P_5 emission over a range $(3 - 7) n_c$ for the first, and between $16 n_c$ and $24 n_c$ for the other. While the feature at the lower densities includes the cold plasma resonance at $4 n_c$, the range of densities spreads across those that generate strong P_3 emission.

Note that, in contrast to the third harmonic, plasma emission around $25 n_c$ is masked by the contribution from the resonance at $16 n_c$. Overall, the result in (10) is a fair representation over the density range $(20 - 40) n_c$ but thereafter significantly underestimates the contribution to P_5 . This underestimate can be attributed at least in part to our neglect of non-resonant terms in the approximation to P_5 in (10). Neglecting these contributions at higher densities is likely to lead to values for P_5 too small by a factor of 2. In the case of the third harmonic, we introduced an artificial damping into the cold plasma model to resolve the resonant denominator. In the same way, the result in (10) may be made to conform to the PIC $(P_5 - n_c)$ plot with its dual resonance structure with finite widths, but this amounts to nothing more than a cosmetic fit with no physical basis. Only by resorting to a more complete model might we hope to properly reproduce the resonant structures in Fig. 4.

We turn instead to a hybrid PIC-theory model using a simple scaling law. This is based on the observation that

the dominant contribution to P_{2m+1} comes from the nonlinear combination of the neighbouring lower order harmonic amplitude a_{2m-1} with a_0^2 . This suggests that P_{2m+1} should scale as

$$P_{2m+1} \simeq \left(\frac{2m+1}{2m-1} a_0^2 \right)^2 P_{2m-1}. \quad (11)$$

By substituting the appropriate PIC results for P_{2m-1} , we can get estimates for P_{2m+1} emission. This is plotted in

TABLE I. Resonant densities for odd harmonic emission.

Harmonic (ω_n/ω_0)	Resonant density (n_e/n_c)	Sources
3	3-6	Spans cold plasma resonance at $4 n_c$.
	9	Plasma emission (strong).
5	3-7	$(a_3 - a_0^2)$ source.
	16-24	Broadened cold plasma resonance at $16 n_c$.
	25	Plasma emission (weak).
7	4-7	Combined $(a_5 - a_0^2)$ and $(a_3 - a_0^4)$ sources.
	11-16	Broadened cold plasma resonance.
	32-36	Broadened cold plasma resonance.
	~ 49	Plasma emission (weak).
9	4-7	Combined $(a_7 - a_0^2)$, $(a_5 - a_0^4)$, $(a_3 - a_0^6)$ sources.
	14-18	Broadened cold plasma resonance.
	30-38	Broadened cold plasma resonance.
	50-60	Source not identified.
	64-69	Cold plasma resonance.
	88	Plasma emission (weak).

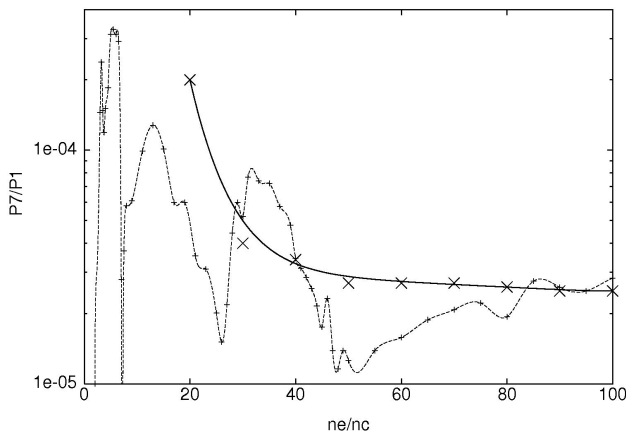


FIGURE 6. Reflected power in the seventh harmonic as a function of n_e/n_c , for $a_0 = 0.5$. The solid line represents a fit to the estimates made using the phenomenological relation (11), marked with points \times . The points $+$ were obtained from PIC simulations.

Fig. 5 along with the PIC data and the cold plasma result as a function of plasma density. From this we see that this scaling law provides a reasonable representation of fifth harmonic emission away from the resonance region.

3.3. Higher order emission

As we proceed to higher harmonic orders, we have little option but to resort to this scaling law approach, since stretching the perturbation expansion to higher orders is as unrewarding as it is laborious. That said, we know enough from low-order perturbation theory to let us extrapolate a result that at least shows the resonant dependence of P_7 on plasma density and on laser intensity, namely

$$\frac{P_7}{P_1} \simeq C_7 \frac{\left(\frac{\omega_0}{\omega_p} \right)^2}{\left(1 - 4 \frac{\omega_0^2}{\omega_p^2} \right)^2 \left(1 - 16 \frac{\omega_0^2}{\omega_p^2} \right)^2 \left(1 - 36 \frac{\omega_0^2}{\omega_p^2} \right)^2} \times \frac{a_0^{12}}{\left(1 + \frac{a_0^2}{2} \right)^9}, \quad (12)$$

in which C_7 is an undetermined factor which we expect to be only weakly dependent on n_e . It is clear from (12) that to this order there is again an additional resonant density in the denominator at $n_e = 36 n_c$.

Figure 6 reproduces our PIC results for P_7/P_1 , showing a clear resonant structure, if not precisely that predicted by (12). As we have noted already for P_5 , strong P_7 emission occurs over a range of density between about $3 n_c$ and $7 n_c$, generated from a $(P_5 - a_0^2)$ source. Moving up in density, we find a second peak in P_7 emission across the range (11-16) n_c . The next feature is a resonance extending over densities (32-36) n_c , corresponding to the additional factor included in the denominator of (12). Included in Fig. 6 are estimates for P_7 found using (11). As noted in Table I, there are two sources for P_7 . The points plotted in Fig. 6 represent only the contribution from the P_5 source. Including that from P_3 increases power in the seventh harmonic by about 30%. Again, this proves to be a surprisingly good representation, confirming the robustness of the scaling in (11). Although resolved, note that P_7 plasma emission is now a weak feature compared with the plasma lines in P_3 , and to a lesser extent, P_5 .

Finally, we can repeat the procedure we have described and obtain an expression for P_9/P_1 :

$$\frac{P_9}{P_1} \simeq C_9 \frac{\left(\frac{\omega_0}{\omega_p} \right)^2}{\left(1 - 4 \frac{\omega_0^2}{\omega_p^2} \right)^2 \left(1 - 16 \frac{\omega_0^2}{\omega_p^2} \right)^2 \left(1 - 36 \frac{\omega_0^2}{\omega_p^2} \right)^2 \left(1 - 64 \frac{\omega_0^2}{\omega_p^2} \right)^2} \times \frac{a_0^{16}}{\left(1 + \frac{a_0^2}{2} \right)^{12}}, \quad (13)$$

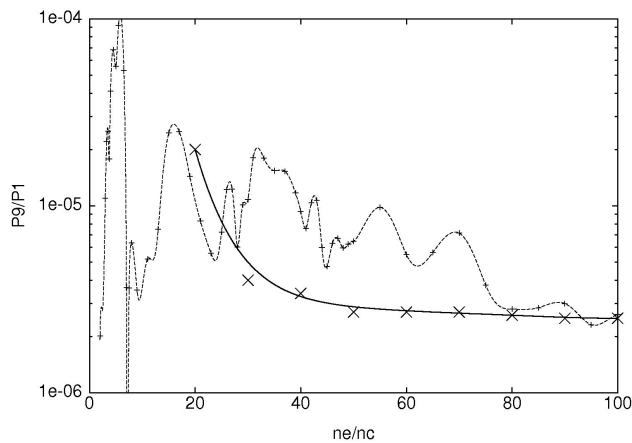


FIGURE 7. Reflected power in the ninth harmonic as a function of n_e/n_c , for $a_0 = 0.5$. The solid line represents a fit to the estimates made using the phenomenological relation (11), marked with points x . The points $+$ were obtained from PIC simulations.

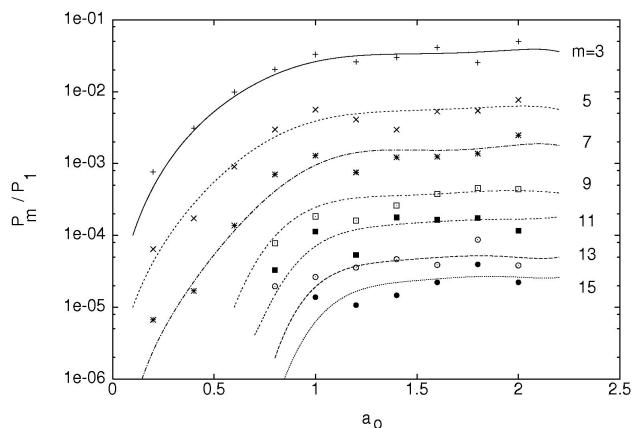


FIGURE 8. Reflected power of laser harmonics as a function of a_0 , for $n_e = 10 n_c$.

with the expected additional cold plasma resonance at $n_e = 64 n_c$. The P_9/P_1 vs n_e/n_c plot in Fig. 7 from our PIC runs shows a richly resonant structure with pronounced resonances across the density ranges shown in Table I. The points x are the estimates of P_9 found using (11). Once again, the scaling provides levels of P_9 emission of the right order, bearing in mind that contributions at resonant densities now affect virtually the entire range. Again we stress that the estimates plotted in Fig. 7 correspond to the principal contribution to P_9 (cf. Table I). Including those from P_5 and P_7 increase P_9 levels across the range by about 50%, which brings the estimated levels of P_9 even closer to the PIC results.

The lowest resonance is again a reflection of the strong P_7 effect over the same density range. The next two peaks include $n_e = 16 n_c$ and $36 n_c$ respectively. Above that, the picture is less clear cut. There is no obvious source for the structure across the range $(50-60) n_c$, although the P_7 plasma line may contribute at the lower end of the range. Note that power levels of P_9 emission at $n_e \sim 55 n_c$ are comparable to those of P_7 (cf. Fig. 6). Further simulations are needed to resolve this anomaly. We interpret the effect at $n_e = 69 n_c$

as the next order cold plasma resonance. The relatively weak emission at $n_e \sim 88 n_c$ may be due to Langmuir wave conversion. In Table I, we summarise the density structure observed in different harmonic orders in this work.

Finally, we show in Fig. 8 the power radiated in odd harmonics up to order 15 as a function of a_0 , from our PIC simulations. As shown in this figure, the laser harmonics are more efficiently produced as the driver field increases in amplitude, generating even more harmonics. As the laser amplitude, continues increasing in amplitude an evident saturation effect characterises the spectrum above laser amplitudes that cause plasma particles to achieve relativistic energies. This saturation effect is a consequence of the increase in energy deposition into particle kinetic energy, thus lowering the conversion efficiencies for power levels in the reflected harmonics.

4. Conclusions

We conclude that, while the behaviour of the power reflected in the various harmonic orders as a function of laser intensity is relatively uncomplicated (cf. Fig. 8), to a degree that allows us to write down a simple scaling with intensity, seen as a function of plasma density its behaviour is altogether more involved. The most striking aspect of the dependence on density is the sequence of resonances predicted by the cold plasma model used in this work and borne out by simulations with a PIC code. Within the resonant range, the reflected power varies by up to an order of magnitude, depending on the density. Only above this range does emission decay inversely with density, as one expects, given the corresponding reduction in electron quiver velocity as the density increases. For low harmonics in the intensity range considered, Langmuir wave-generated radiation contributes to the emission overall. However, at higher densities its contribution is relatively less significant, at least in this weakly driven regime, decreasing approximately as n_e^{-2} .

Finally, is any of this density dependence observable for a particular harmonic? The difficulty faced here is that of creating target plasmas over a sufficient range of density to explore the behaviour of, for example, P_5 in the range $(10-30) n_c$ to determine whether or not the variation in intensity predicted by our analysis does indeed occur. One should also bear in mind that these predictions are based on the assumption that the target is a plasma slab with a step in density at the boundary. The presence of a finite density gradient at the plasma surface might be expected to diminish the scale of the variation in the intensities of particular harmonics with density.

Acknowledgments

One of us (TJMB) acknowledges partial support for a visit to ININ enabling the work described in this paper to be completed. Financial support from Consejo Nacional de Ciencia y Tecnología (CONACyT) under Contract No. 43621-F is also acknowledged by ROR.

-
1. N.H. Burnett *et al.*, *Appl. Phys. Lett.* **31** (1977) 172.
 2. R.L. Carman, C.K. Rhodes, and R.F. Benjamin, *Phys. Rev. A* **24** (1981) 2649.
 3. P.A. Norreys *et al.*, *Phys. Rev. Lett.* **76** (1996) 1832.
 4. P. Gibbon, *Phys. Rev. Lett.* **76** (1996) 50.
 5. P. Gibbon, *J. Quant. Electronics* **33** (1997) 1915.
 6. S. Gordienko *et al.*, *Phys. Rev. Lett.* **93** (2004) 115002.
 7. R. Ondarza, *Phys. Rev. E* **67** (2003) 066401.
 8. T.J.M. Boyd and R. Ondarza-Rovira, *Phys. Rev. Lett.* **85** (2000) 1440.
 9. S.C. Wilks, W.L. Kruer and W.B. Mori, *IEEE Trans. Plasma Sci.* **21** (1993) 120.
 10. R. Ondarza-Rovira, Ph. D. Thesis, University of Essex, UK, (1996).
 11. P. Sprangle, E. Esarey, and A. Ting, *Phys. Rev. A* **41** (1990) 4463.
 12. P. Sprangle and E. Esarey, *Phys. Fluids B* **4** (1992) 2241.